The finite-volume time-domain method for 3-D solutions of Maxwell's equations in complex geometries: a review

Christophe Fumeaux[1], Dirk Baumann[2], Krishnaswamy Sankaran[1], Klaus Krohne[2], Rüdiger Vahldieck[1] and Erping Li[2]

Abstract – This paper reviews the recent advances of finite-volume techniques applied to the solutions of Maxwell's equations, placing emphasis on the microwave engineering perspective. The theoretical foundations, as well as variations of cell-centered finite-volume algorithms are described together with the modules necessary for the practical application of the method. The main advantage of finite-volume algorithms is their applicability to unstructured meshes, which provides great geometrical flexibility for modeling complex electromagnetic problems. As a 3-D simulation example, the coupling between two Archimedean spiral antennas is presented, illustrating the outstanding capabilities of the method but also addressing the associated computational costs. Weighting the strengths and drawbacks of the finite-volume time-domain method, a summary of its potential is given in the conclusion of the paper.

Index Terms – Computational electromagnetics (CEM), Time domain analysis, Frequency domain analysis, Finite-Volume Time Domain (FVTD) method.

I. Introduction

The continuous advancement of microwave circuits and electromagnetic devices towards increased functionality and performance requires simultaneous development of design tools that are able to keep up with the increased level of sophistication in circuit design and realization. This need has fueled the progresses of electromagnetic simulation codes, which have been furthermore empowered by the spectacular development of computing hardware. As a result, electromagnetic simulations of structures with increasing size and complexity become feasible using off-the-shelf personal computers and general-purpose field solvers. Among the computational algorithms that are applied to the solution of electromagnetic problems, the Finite-Difference Time-Domain method (FDTD), the Finite-Element Method (FEM), the variations of the Method of Moments (MoM), and the Transmission Line Method (TLM) can be mentioned as some of the more prominent examples. Efforts are still made to bring improvements to those numerical techniques, as no single method can claim a global superiority in efficiency and accuracy for all problems encountered in the multitude of today's electromagnetic systems. Therefore, the coexistence of various algorithms is essential to widen the range of standard and non-standard problems that can be simulated with practical relevance. In this perspective, besides advances in the mainstream algorithms, investigations of less established methods represent an alternative way of expanding the capabilities of numerical electromagnetic modeling. This paper describes the investigations of one of the less known techniques, the Finite-Volume Time-Domain (FVTD) method. It reviews the present state of the research and addresses the potential of the method for engineering applications either as stand-alone, or in hybrid implementations.

The FVTD method has been introduced at the very end of the 1980's [1][2] as a powerful technique to solve Maxwell's equations. It takes its inspiration from the finite-volume techniques that are used to solve the governing equations of fluid dynamics in their conservative form. The FVTD method is characterized by a great geometrical flexibility since it can be applied in unstructured polyhedral meshes. While other elementary shapes are conceivable, the method is commonly implemented in tetrahedral meshes, which permits to model complex structures with great fidelity. Therefore, the most obvious advantage of the FVTD unstructured mesh arises from the conformal approximation of curved and slanted surfaces. However, an even more relevant advantage comes from the possibility to locally adapt the size of the finite-volume cells to the geometrical features of the modeled structures. This is beneficial for instance, for the modeling of structures with large dielectric contrasts: Materials with a large dielectric permittivity can be discretized with smaller cells than lower permittivity materials, bearing in mind that spatial discretization needs to be a small fraction of the wavelength in the medium ($\leq \lambda_\varepsilon/10$). Furthermore, the resolution of small structural details (e.g. with features in the order of $\lambda_\varepsilon/100$) embedded in larger objects also benefits from an inhomogeneous mesh to minimize the number of cells in the discretized model. In all cases, the transition from smaller to larger cells can be realized smoothly using an unstructured mesh. The local mesh refinements are naturally incorporated in the FVTD algorithm, and therefore, the complexity of the simulation is reduced to a meshing problem. Since the FVTD method combines the flexibility of an unstructured mesh with the advantages of an explicit time-domain method, it can be considered somewhat halfway between the FEM and the FDTD method.

This paper reviews the investigations performed by the authors on the FVTD method during the last few years. Sect.

Received February 26th, 2007 . Revised March 26th, 2007.

[1]Laboratory for Electromagnetic Field Theory and Microwave Electronics, ETH Zurich, Zurich, CH-8092, Switzerland.
E-mail: fumeaux@ifh.ee.ethz.ch;
[2]Electromagnetic Department, Institute of High Performance Computing, A*STAR, Singapore 117528.

2 gives a brief description of the basics of the algorithm, placing the emphasis on the physical interpretation rather than on the mathematical treatment. Based on the fundamental finite-volume integral equations, many numerical implementations are possible. Some of the most common variations in the algorithm are described in Sect. 3, together with a brief discussion on the frequency-domain implementation of the algorithm. Section 4 describes specific implementation requirements relevant for a practical application of the FVTD method to microwave engineering problems. Later, as an illustration, the challenging example of the mutual coupling between two cavity-backed Archimedean spiral antennas is presented in Sect. 5. For validation, the simulation results are compared with measured data. In the conclusion, the paper assesses the advantages and drawbacks of the FVTD method as a general-purpose electromagnetic field solver. More generally, it predicts the potential of conformal time-domain methods in the future landscape of electromagnetic simulation tools.

II. FVTD fundamentals

The FVTD method is based on Maxwell's curl equations written in a conservative form [3] and integrated over a finite-volume [4]:

$$(1)\qquad \begin{aligned} -\frac{\partial}{\partial t}\iiint_V \vec{B}\,dv &= \oiint_{\partial V} \vec{n}\times\vec{E}\,da \\ \frac{\partial}{\partial t}\iiint_V \vec{D}\,dv &= \oiint_{\partial V} \vec{n}\times\vec{H}\,da. \end{aligned}$$

This system of equations relates integrals over the volume V to surface integrals over the boundary ∂V of V. The integrand on the right-hand side (RHS) is called the "flux" through the boundary surface ∂V and is constructed using the outward-pointing normal vector $\vec{n}$ on each infinitesimal surface element da. In the original fluid dynamics interpretation, the system of equations (1) considers the variation of conserved quantities in a given volume (left-hand side - LHS) that is compensated by fluxes through its boundary surface (RHS). It is also remarkable that only the tangential field components on the closed surface ∂V are relevant in the exchange of information between the volume V and its surroundings, which is in accordance to the uniqueness theorem of electromagnetic fields.

The numerical implementation of the fundamental FVTD equations requires the discretization of the system (1) in space and time. The spatial discretization is obtained by partitioning the computational domain into elementary polyhedral cells. The cell with index i is characterized by its volume, denoted as V_i, and by its boundary surface ∂V_i, which is composed of N_i faces. Each polygonal face of the polyhedral cell is characterized by its area F_k and its outward-pointing normal vector $\vec{n}_k$ ($k = 1, ..., N_i$). Under the assumption that the cell i has homogeneous permittivity ε_i and permeability μ_i, the system of equations (1) can be written in a discrete form as

$$(2)\qquad \begin{aligned} -\mu_i V_i \frac{\partial}{\partial t}\left\langle \vec{H}\right\rangle_{V_i} &= \sum_{k=1}^{N_i}\left(\vec{n}_k \times \left\langle \vec{E}\right\rangle_{F_k}\right) F_k \\ \varepsilon_i V_i \frac{\partial}{\partial t}\left\langle \vec{E}\right\rangle_{V_i} &= \sum_{k=1}^{N_i}\left(\vec{n}_k \times \left\langle \vec{H}\right\rangle_{F_k}\right) F_k \end{aligned},$$

where the bracketed values $\langle\cdot\rangle$ indicate spatially averaged values, either over the volume V_i (LHS) or over the surface F_k (RHS). Although discretized, this set of finite-volume equations (2) is still exact, providing the spatially averaged values are known exactly. However in practice those average values are only found through approximations, which introduce numerical errors in the algorithm.

III. Algorithm variations

Many variations in the finite-volume algorithm for the system (2) exist, depending on the choice of variable location in the cells. Among all possibilities, the discussion here is restricted to the class of spatially collocated cell-centered algorithms. Those are characterized by the location of all components of both the $\vec{E}$ and $\vec{H}$ field in the barycenters of the volumes. For the elementary cell i, this can be expressed as the following approximation

$$(3)\qquad \left\langle \vec{H}\right\rangle_{V_i} \approx \vec{H}_{BC,i} \triangleq \vec{H}_i \text{ and } \left\langle \vec{E}\right\rangle_{V_i} \approx \vec{E}_{BC,i} \triangleq \vec{E}_i,$$

where the subscript BC indicates the barycenter location. This approximation is only meaningful for elementary cells with dimensions corresponding to a small fraction of the wavelength λ_ε in the considered medium. Accordingly, the averaged field vectors on the face k are approximated by the values in the face center (denoted by the subscript FC)

$$(4)\qquad \left\langle \vec{H}\right\rangle_{F_k} \approx \vec{H}_{FC,k} \triangleq \vec{H}_k \text{ and } \left\langle \vec{E}\right\rangle_{F_k} \approx \vec{E}_{FC,k} \triangleq \vec{E}_k.$$

Considering the class of cell-centered finite-volume algorithms of interest here, the numerical computation of the fluxes $\vec{n}_k \times \vec{E}_k$ and $\vec{n}_k \times \vec{H}_k$ on the face centers of the elementary cells provides additional room for different approximation strategies. Some frequently used techniques are briefly described in the following, addressing their advantages and disadvantages.

A) Flux-splitting algorithm

The flux-splitting algorithm has been adapted in [2] for Maxwell's equations. It decomposes the total flux across a face into incoming and outgoing fluxes. This separation is based on the method of characteristics with solutions propagating with velocities given by the eigenvalues of the Jacobian matrix of the system [5],[6]. This can be interpreted as decomposing the field into plane waves that are propagating normally to the cell faces. The finite-volume

equation can then be written as

$$(5)\qquad \begin{aligned} -\mu_i V_i \frac{\partial \vec{H}_i}{\partial t} &= \sum_{k=1}^{N_i} \left(\vec{n}_k \times \vec{E}_k^{+} + \vec{n}_k \times \vec{E}_k^{-} \right) F_k \\ \varepsilon_i V_i \frac{\partial \vec{E}_i}{\partial t} &= \sum_{k=1}^{N_i} \left(\vec{n}_k \times \vec{H}_k^{+} + \vec{n}_k \times \vec{H}_k^{-} \right) F_k \,. \end{aligned}$$

The superscripts $+$ and $-$ on the RHS of the equation mark the field components associated with the outgoing and incoming fluxes, respectively. The outgoing fluxes are computed based on the barycenter field values in the considered cell i, whereas the incoming flux through face k is obtained from the field values in the neighboring cell j sharing the face, as depicted schematically in Fig. 1(a). The reader is referred to [3],[7] for a detailed mathematical description of the flux-splitting algorithm.

To improve the approximation to second-order accuracy, the Monotone Upstream-centered Scheme for Conservation Law (MUSCL) [8] is generally applied together with this flux-splitting algorithm. The MUSCL improves the approximation of the face center values $\vec{E}_k^{+}$, $\vec{E}_k^{-}$, $\vec{H}_k^{+}$ and $\vec{H}_k^{-}$ by using the gradient information of each field components inside the cell (linear approximation).

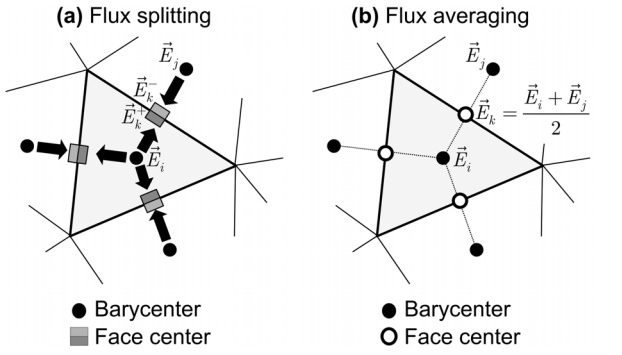

Fig. 1. Schematic representation of the computation of the fluxes (a) Flux splitting, (b) Flux averaging. Only selected E-field vectors are indicated for clarity.

To obtain explicit update equations, the time derivative on the LHS of (5) is discretized using standard techniques such as the Lax-Wendroff predictor-corrector scheme [9] or a Runge-Kutta type integration scheme.

The flux-splitting algorithm provides a robust update equation for the FVTD time-stepping iteration. The treatment of boundaries is naturally incorporated in the algorithm, and the method shows a low level of numerical dispersion (phase error). However, it must be mentioned that the algorithm shows a dissipative behavior because of the upwind approximation of fields on the face centers [10]. This dissipation is a drawback of the method, which becomes apparent for coarser spatial discretizations. In broadband simulations, this degrades the results at the higher end of the frequency spectrum, where the mesh becomes coarser with respect to the wavelength. For the flux-splitting algorithm, the dissipation, besides the geometric features to be resolved by the mesh, sets the basic requirement of a sufficiently fine spatial discretization in order to obtain a satisfying convergence in the solution. In particular, dissipation may compromise the accuracy of results in the simulation of resonant devices.

B) Flux-averaging algorithm

The flux-averaging algorithm has been introduced in [11] as a non-dissipative finite-volume scheme. The field values on the cell faces, necessary to compute the fluxes on the RHS of the FVTD equations (2), are obtained as a simple average of the two barycenter values of the neighboring cells. This can be written as

$$(6)\qquad \begin{aligned} -\mu_i V_i \frac{\partial \vec{H}_i}{\partial t} &= \sum_{k=1}^{N_i} \left(\vec{n}_k \times \frac{\vec{E}_i + \vec{E}_j}{2} \right) F_k \\ \varepsilon_i V_i \frac{\partial \vec{E}_i}{\partial t} &= \sum_{k=1}^{N_i} \left(\vec{n}_k \times \frac{\vec{H}_i + \vec{H}_j}{2} \right) F_k \,. \end{aligned}$$

In this system, j is used as a subscript for the vector field values in the barycenter of the neighboring cell of i sharing the face k, as depicted in Fig. 1 (b). The spatial approximation is combined with a leap-frog time discretization in order to obtain a fully explicit time-stepping scheme. The scheme has been proven to be non-dissipative, and validation examples have been proposed for 2-D in unstructured triangular meshes and for 3-D in structured hexahedral meshes [11]. The non-dissipative behavior is achieved at the cost of an increasing numerical dispersion (similarly to FDTD). However, the general applicability of the scheme seems very limited. First, spurious oscillations are observed in unstructured grids [12]. Second, the scheme exhibits grid decoupling effects that are directly observable in 2-D implementation: A line source excitation in a cell barycenter affects the H-field in the neighboring cells, however the E-field only in the second next neighbor. This results in a checkerboard pattern for a square grid, and in a patched pattern for a triangular mesh. This can be intuitively understood considering that the method is staggered in time (leap-frog), but collocated in space. Finally, additional attempts by the authors to implement the scheme in a 3-D tetrahedral mesh have yielded unsatisfactory results.

C) $\beta\gamma$-Schemes

A compromise can be made by combining the dissipative flux-splitting and the non-dissipative (but dispersive) flux-averaging schemes through the so-called β-schemes [13],[14]. This basically corresponds to a weighted average between the two previously presented schemes. An extension to this concept is given by the $\beta\gamma$-scheme described in [15], which uses two parameters to obtain a better control of the tradeoff between dissipation and dispersion. This class of schemes however has not found a widespread acceptance because of the difficulty to determine general control parameters valid for any mesh. This represents a drawback that is especially relevant for 3-D tetrahedral meshes, since no guarantee exists that a set of parameters will yield meaningful results.

D) Frequency domain algorithms

While time-domain implementations have been able to deliver outstanding results for broadband devices, the investigation in frequency-domain appears to be attractive when considering narrowband and/or resonant devices for which the long settling times along with the previously mentioned dissipation can render the application of a time-domain solver futile. However, as opposed to the traditional time-domain implementations of the finite-volume technique, which rely on an update scheme, where every time step requires looping through all the cells of the computational domain, a frequency-domain solution demands a matrix formulation. Such a formulation in terms of a state-space system has been introduced recently for the flux-splitting [16] as well as the flux-averaging [17] scheme.
If the individual components of the electric and magnetic fields are collected in the state-vector $\mathbf{X}$, (2) can be directly transformed into

$$s\mathbf{X} = \mathbf{A}\mathbf{X} + \mathbf{B}\mathbf{x}(s). \tag{7}$$

where s is the complex frequency and $\mathbf{A}$ is referred to as the system matrix. Each row of $\mathbf{A}$ computes the time derivative of one field component in one cell referring to the cell itself and its surrounding neighbors. Thus, it has to perform inter- or extrapolation, compute the cross-product with the respective normal vector and the product with the interface area, and sum the result of the faces that compose a particular cell. Together with the output equation

$$\mathbf{y}(s) = \mathbf{C}\mathbf{X} + \mathbf{D}\mathbf{x}(s), \tag{8}$$

where $\mathbf{B}$ and $\mathbf{C}$ are port operators that map the input and output vectors $\mathbf{x}$ and $\mathbf{y}$ to the computational domain, equations (7) and (8) form the standard state-space formulation for linear time invariant (LTI) multi-input multi-output (MIMO) systems. A feedthrough $\mathbf{D}$ may be present, depending on the scheme that is being deployed.
The system's transfer function can be computed by solving (7) for $\mathbf{X}$ and placing it into (8). It then depends on the nature of the input and output quantities $\mathbf{x}$ and $\mathbf{y}$ whether the transfer function is the device's scattering matrix or its impedance matrix. Since the flux-splitting scheme gives access to the individual incoming and outgoing wave amplitudes, the result of a frequency-domain solution is a scattering matrix, whereas the flux-averaging scheme yields the total fields on the port faces, which are related to the generalized port currents and voltages. For this reason, if the flux-averaging scheme is applied, a frequency-domain solution of (7) and (8) results in the device's impedance matrix. In that case the feedthrough $\mathbf{D}$ vanishes.
The computational load lies in the solution for the state vector $\mathbf{X}$ from (7). The solution is reasonably efficient for small scale problems, where a full LU decomposition of the left-hand side $(s\mathbf{I} - \mathbf{A})$ is possible. Large problems require the application of iterative solvers, which, due to the high condition number of $(s\mathbf{I} - \mathbf{A})$, tend to suffer from slow convergence.
An approach to combine the superior shape approximation capabilities of the finite-volume method with the efficiency of a frequency-domain solver for resonant devices is the application of a two-step model order reduction (MOR) technique [18] as demonstrated in [19].

IV. Practical implementation

In the following, the important aspects for a FVTD simulation with practical relevance in microwave engineering are described. The flux-splitting algorithm described in Sect. III A) is used in this framework, although most of the practical implementations shown in this section can be employed in other formulations too. The simulation example, that follows in Sect. V, is also computed using the flux-splitting algorithm which has proven to be the most robust FVTD algorithm of its class.

A) Mesh generation, mesh quality

Tetrahedral meshes typically constitute a very convenient discretization for FVTD simulations as they provide an unmatched flexibility for conformally approximating complex structures. In addition, mesh generators that provide high-quality tetrahedral meshes have been developed in several engineering areas and are readily available. A tetrahedron is deemed to be of good quality if it is nearly regular, i.e. if its edges are all approximately of equal length. The quality of the mesh is crucial for an accurate and efficient FVTD simulation for two reasons:
1. Stability criterion: The stability criterion of an explicit method determines the maximum usable time step Δt for stable iteration and it is given by the famous Courant–Friedrich–Lewy (CFL) condition known from finite-difference methods. For the FVTD method, an equivalent criterion is obtained from the minimum volume-to-surface ratio taken over all the cells

$$t \leq \frac{1}{c} \min_i \left(\frac{V_i}{\sum_{k=1}^{N_i} F_k} \right) \quad . \tag{9}$$

A regular tetrahedron exhibits an optimal volume-to-surface ratio for a given volume. Therefore, a mesh of nearly regular tetrahedrons permits to run the FVTD march-in-time with a larger step than a mesh composed of strongly irregular tetrahedrons of similar volumes.
2. Accuracy: The approximation of the volume integral (3) and surface averages (4) using the value in the barycenters degrades for irregular shapes. Flat or needle-shaped tetrahedral cells increase the mesh-induced numerical noise and negatively affect the spatial convergence of the algorithm. As an empirical rule of thumb, using an irregular cell - with a shortest edge length ℓ_{min} that is much smaller than the longest edge ℓ_{max} - does not improve the convergence of the solution compared to a regular tetrahedron with edge length ℓ_{max}, despite the fact that the irregular cell has a much smaller volume.

B) Material boundaries

The material boundaries are taken into account naturally in cell-centered FVTD algorithms, since the interfaces between media correspond to cell faces. For example, the implementation of the perfect conducting surfaces is straightforward, since the associated boundary conditions correspond to nulling fluxes

$$(10)\quad \begin{array}{l} \text{Perfect electric conductor (PEC):} \quad \vec{n}_k \times \vec{E}_k = 0 \\ \text{Perfect magnetic conductor (PMC):} \quad \vec{n}_k \times \vec{H}_k = 0\,. \end{array}$$

In addition to the standard usage, PEC and PMC surfaces are employed when exploiting symmetries in order to reduce the computational volume.

C) Domain truncation

In any volume-discretization technique, reflection-free domain truncation is indispensable to handle open problems (radiation and scattering). For this purpose, accurate absorbing boundary conditions (ABC) have been developed, which can reduce the unphysical numerical reflections from the outer computational boundary, with the goal of mimicking extension of space to infinity. A common domain truncation that is used in conjunction with the FVTD method is the Silver-Müller ABC (SM-ABC). In the FVTD implementation, the SM-ABC requires setting the incoming fluxes to zero at the outer boundary. However, it is only first-order accurate in space, and performs at its best when the incident wave is normal to the truncating boundary. Hence, in order to achieve good performance for radiation problems, the boundary of the FVTD domain is shaped in the form of a sphere around the simulated structure. If the radius of the sphere is large enough, the shape of the (asymptotically spherical) phase fronts of the radiated fields matches the outer boundary, satisfying the near-normal incidence condition. Therefore, despite its first-order accuracy, the SM-ABC permits to achieve sufficient performance for many engineering applications.

The principle of perfectly-matched layers (PML) that has been introduced by Bérenger [20] in 1994 has revolutionized the treatment of domain truncation. Since then, many different implementations have been proposed for adapting the technique to the FDTD method. Recently, investigations on adapting the Bérenger PML techniques to the FVTD method have been reported in [21],[22]. The absorber model is accurately characterized based on the control parameters, namely absorber thickness, loss-profile, maximum loss and spatial discretization. The optimal values for these parameters were found by studying the performance of the absorber on a 2-D structured triangular mesh. The reflection coefficient as a function of the angle of incidence, obtained from numerical experiments, is represented in Fig. 2. At normal incidence, both the SM-ABC and the FVTD-PML exhibit comparable performance (∼-50 dB). When the angle of incidence is gradually increased away from normal, a degradation of the absorption is noticed. However, for all angles of incidence, the FVTD-PML clearly outperforms the SM-ABC.

The idea of uniaxial PML was extended to radial PML in FVTD [23] to avoid the corner regions encountered in standard FDTD-PML implementations. The direction of wave attenuation inside the absorber is given by the direction of the anisotropy. For the uniaxial absorber this direction is chosen along a particular direction (x, y or z axis). In the case of radial absorber, the anisotropy is chosen along the radial direction. Update equations are derived using a transformation from the locally uniaxial to the globally radial absorber characteristics.

Further PML models like complex-frequency shifted PML (CFS-PML), Lorentz material based absorber etc, have been investigated in the framework of the FVTD method. Theoretical analysis and numerical experiments confirmed similar performance for all PML models studied [24].

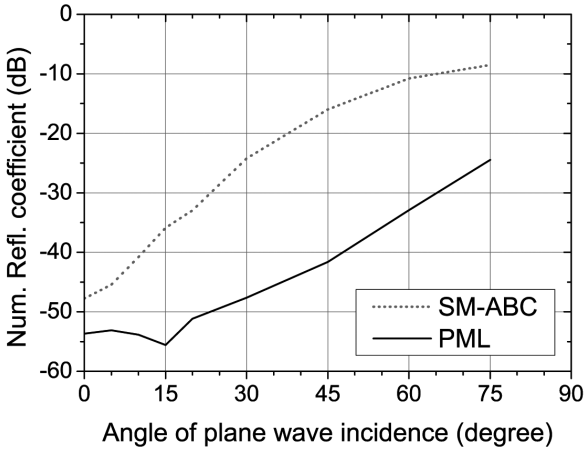

Fig. 2. Comparison of the reflection coefficient as a function of the angle of incidence for a plane wave impinging on an SM-ABC and a PML domain truncation.

D) Port definition

Ports play a crucial role for the simulation of electromagnetic devices, since they provide a defined way of impressing energy into the system, and permit the extraction of scattering parameters. As an additional challenge, ports in certain configurations have to feature a reflection-free truncation of the computational space. Two main aspects characterize the port definition in the FVTD method: First, a port plane defining a phase reference must be introduced in the unstructured mesh. Second, the flux-splitting algorithm described in Sect. III A) is exploited for excitation as well as for a field-based extraction of the scattering parameters without the need of computing additional network parameters [7]. In the following, these two aspects are addressed.

Two ways of creating a port plane in FVTD are illustrated in Fig. 3 for the case of a rectangular waveguide. The first possibility is to introduce a discretized plane in the mesh,

forcing the adjacent tetrahedrons to be aligned in a common plane located either on the computational boundary or in the computational bulk (Fig. 3(a)). This procedure assures a well-defined location of the port plane and enables the use of the readily available field values on the triangular faces of the port. The second way to create a port is to define a virtual port plane by a set of regularly spaced interpolation points at an arbitrary location in the mesh (Fig. 3(b)). This offers a greater flexibility, since the location of the port can be changed without the need of remeshing. The drawback is that an interpolation of the field values onto the port plane becomes necessary.

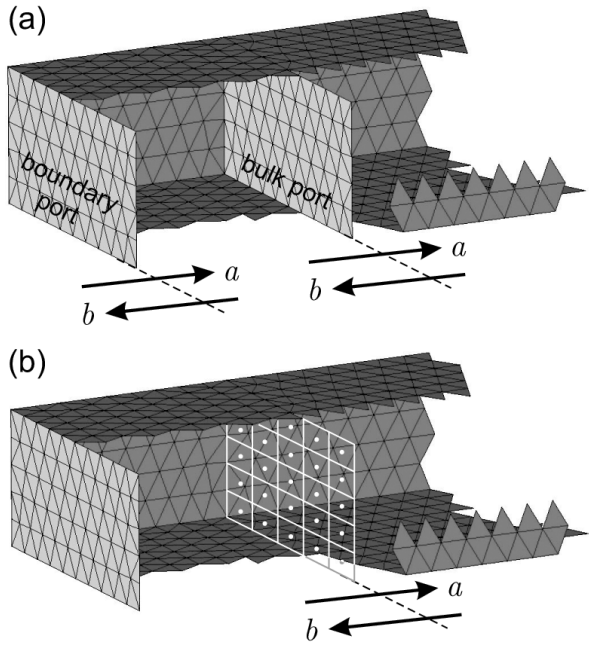

Fig. 3. Port definition in FVTD: The port plane can be introduced as (a) a meshed surface, or (b) as a virtual plane consisting of interpolation points.

The incident wave a, and the reflected wave b through the port plane are connected to the incoming and outgoing fluxes. This fact is exploited to accomplish the multifunctionality of the ports in FVTD:

- In order to impress energy in the port, a mode-template vector is imposed on the incoming fluxes creating a well-defined incident wave.
- In a similar manner, the port plane can be used to truncate the computational domain with a SM-ABC condition by forcing the incoming fluxes to zero, as described in Sect. IV C).
- In the context of scattering matrix extraction, the flux-splitting algorithm is applied on the fields $\vec{E}_k$ and $\vec{H}_k$ in the port plane. However, the split fluxes, as introduced in (5), are corrected with a factor ξ_p dependent on the port mode p. The corrected outgoing $(+)$ and the incoming $(-)$ flux $\vec{\varphi}^{E+/-}$ can then be written as [7]

$$\begin{aligned}\vec{\varphi}^{E+/-} &= \vec{n}_k \times \vec{E}_k^{+/-} \\ &= \frac{1}{2}\left(\vec{n}_k \times \vec{E}_k \pm \vec{n}_k \times \left(\vec{n}_k \times \xi_p \eta \vec{H}_k\right)\right).\end{aligned} \tag{11}$$

The introduction of the correction factor ξ_p is necessary in order to reveal the mode information, which is lost because of the plane-wave character of the split fluxes. The corrected fluxes are solely used for the computation of the scattering parameters – therefore they do not narrow the generality of the core FVTD algorithm. The correction factor is known implicitly from the mode template vectors that are used in the scope of the excitation. Eventually, the total tangential electric fields of the incident wave a and the reflected wave b can be computed from the corrected fluxes (11) according to

$$\begin{aligned}\vec{E}^b &= -\vec{n} \times \vec{\varphi}^{E+} \\ \vec{E}^a &= -\vec{n} \times \vec{\varphi}^{E-}.\end{aligned} \tag{12}$$

In a multi-mode environment, the orthogonality of the modes together with the knowledge of the mode-template vectors enable the determination of the mode amplitudes, and consequently the computation of the generalized scattering matrix [7].

E) Advanced features

The stability criterion in (9) essentially states that the "worst" cell in the mesh determines the pace of the FVTD time iteration. When considering a good quality mesh with nearly regular tetrahedrons, the smallest cell determines the fundamental time step Δt. Therefore, when extremely small cells are required to resolve details of a structure, the efficiency of the computation suffers from a march-in-time with correspondingly short time step Δt. To relax the requirement set by a single stability criterion applied over the whole mesh, a local time-stepping scheme has been presented in [25]. The proposed technique is based on an automatic partitioning of the computational domain into sub-domains, where local time steps equal to power-of-two multiples of the fundamental time step Δt are applied, i.e. Δt,$2\Delta t$,$4\Delta t$, …, $2^{n-1}\Delta t$. During the march in time that is performed with the fundamental time step Δt, the update is performed selectively according to the sub-domain, e.g. cells in a sub-domain with local time-step $4\Delta t$ will be updated only every 4^{th} iteration step. Limiting the jump at all interfaces between sub-domains to a factor of two in Δt allows implementing a generalized, accurate and robust two-level connection between sub-domains. Depending on the problem, the local time stepping procedure was found to typically speed up the computation by a factor of 2 to 5.

Other techniques have been proposed to improve the efficiency of the computation for specific problems. Among the specialized techniques, the wire model of [26] and the FVTD/FDTD hybridization of [27] can be mentioned.

V. Application example

The simulation of the coupling between two Archimedean spiral antennas is presented in the following as an illus-

tration of the capability of the FVTD method to model extremely complex geometries. The Archimedean spiral antenna is characterized by a fixed arm width and operates with stable input impedance and radiation characteristics over a wide bandwidth. The frequency range of circular polarized radiation is determined by the inner and outer radii of the spiral. For most applications unidirectional radiation is strongly desired and hence spiral antennas are often backed by an absorber-loaded cavity that provides broadband suppression of the back radiation. A detailed FVTD simulation of a cavity-backed Archimedean spiral antenna for 2-18 GHz has been presented in [28]. The most challenging aspect is the modeling of the two spiral arms that extend over 26 windings, and therefore exhibit a high contrast between the arm width of 0.25 mm and the total arm length of more than 2 m. In addition, by employing a highly inhomogeneous mesh, the 0.25 mm thin substrate, the balun and the honeycomb absorber in the cavity can be incorporated in the FVTD model. Comparisons of simulations with measured data have shown excellent agreement [28].

In the following, the coupling between two of such Archimedean spiral antennas located in close proximity is investigated. The first configuration considers both spirals placed in a common plane as shown in Fig. 4. Both the spirals are identical to the one presented in [28], except for the fact that the honeycomb absorber has been replaced by an ABC that provides a simplified model of the absorber. The spiral has an outer radius of 26 mm, and is mounted on the metallic cavity with an external diameter of 62 mm and a height of 37 mm. The spiral on the LHS is excited through the coaxial port of the balun using a broadband modulated Gaussian pulse (2-18 GHz), and the response is registered in the coaxial port of the balun of the spiral on the RHS in Fig. 4.

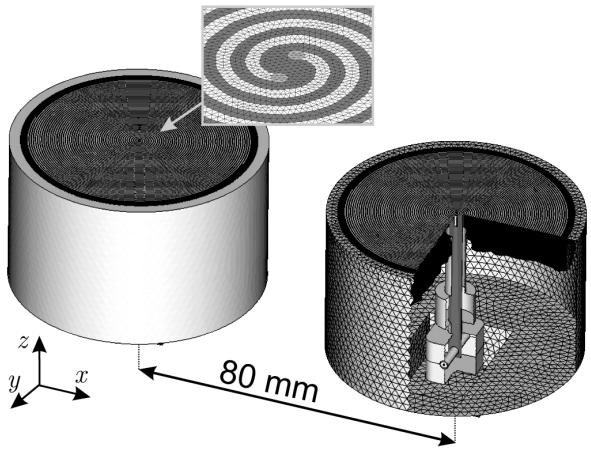

Fig. 4. Configuration of the two spirals in a common plane. The spiral on the RHS is displayed with part of its surface mesh and is cut open to reveal the balun and the cavity. The inset shows the detail of the mesh spiral around the center of the LHS spiral.

The coupling parameter S_{21} computed in the FVTD simulation is shown as a function of the frequency in Fig. 5, and compared to measured data. Considering on one hand the low-level of the coupling between the antennas, and on the other hand the complexity of the problem, the agreement between the numerical and measured data is excellent. Some of the ripples observed in the simulated S_{21} can be explained through low-level reflections from the SM-ABC truncation that is employed in this example. Based on this result, it is clear that the general behavior of the coupling can be fully and accurately predicted through numerical simulation. Further analysis (not shown here for brevity) at different distances exhibit a comparable agreement between simulation and measurement, which further demonstrates the robustness of the method.

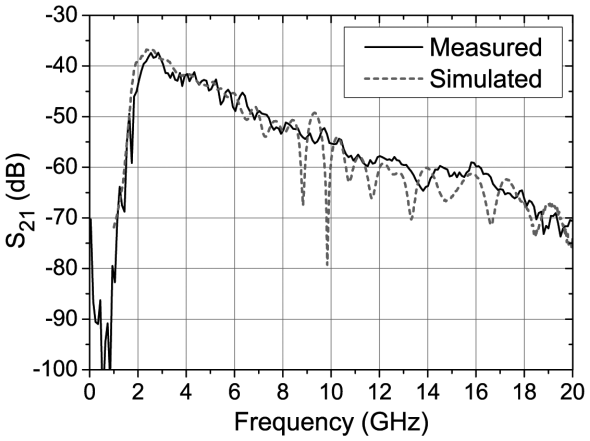

Fig. 5. Coupling parameter S_{21} of the two spirals in the configuration of Fig. 4. The graph compares the results obtained from the FVTD simulations with measured data.

A second effect of the coupling is manifested by the modification in the radiation patterns of the active antenna in the presence of the second antenna. Because of the low level of coupling, this effect is expected to be weak, consequently providing a way of testing the sensitivity of the numerical method. The radiation pattern of the spiral with and without the second spiral in close proximity is shown in Fig. 6. For illustration, the frequency is chosen at 10 GHz, i.e. at the center of the operating range, but similar results are also found at other frequencies. The patterns are shown in the *xz* plane (as defined in Fig. 4) where the effect of the second spiral is most visible. The upper graph of the figure (Fig. 6(a)) compares measured and simulated patterns for a single spiral in free-space. The center graph (Fig. 6(b)) shows the corresponding patterns for the case, when the spiral is operated in the presence of the in-plane second spiral in the configuration of Fig. 4. The agreement between simulation and measurement is excellent for both cases. Based on this agreement, the comparison of the patterns with and without the second spiral is then shown for simulated data only in Fig. 6(c). The second spiral diffracts radiation of the excited antenna and causes a small indentation in the pattern at about 90 degree, i.e. at the location of the second spiral. This effect is observed both in simulation and measurement.

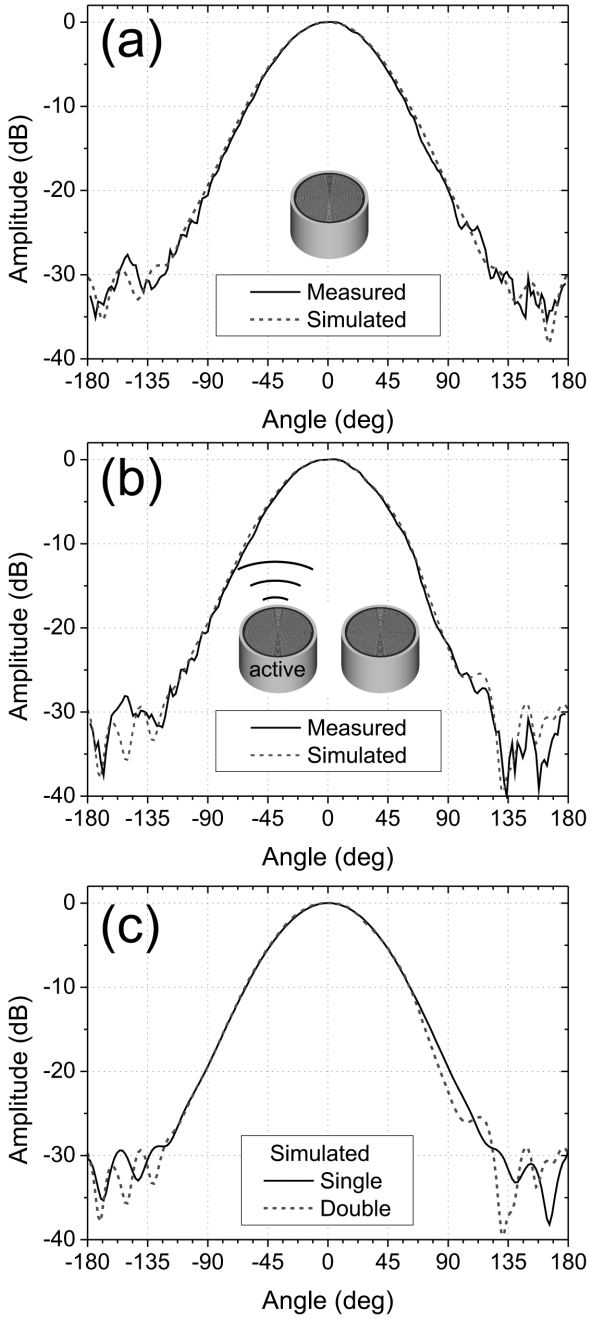

Fig. 6. Patterns of the spiral antenna at 10 GHz. (a) Comparison of simulated and measured pattern for a single spiral in free-space. (b) Comparison of simulated and measured pattern for a double spiral configuration (Left-hand spiral is active). (c) Comparison of simulated patterns for single spiral in free-space and for in-plane double spiral configuration.

Although the simulation of the two spirals in the in-plane configuration represents a very challenging example for any numerical method, the difficulty is further increased for Cartesian grids when the spirals are tilted as shown in Fig. 7. For the FVTD models, since there are no preferred directions in the unstructured tetrahedral mesh, the computational cost of the tilted configuration is identical to the in-plane configuration.

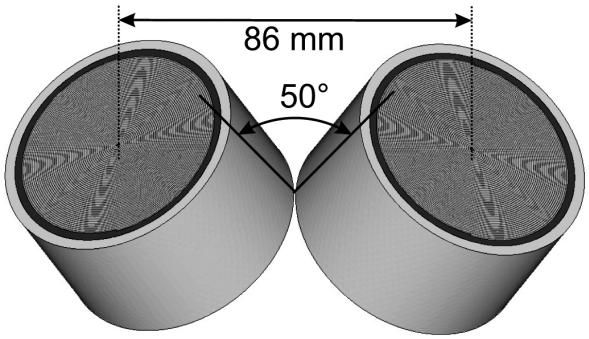

Fig. 7. Configuration of the two spirals in tilted configuration. Both spirals are rotated as shown, and the spiral enters are separated by a distance of 86 mm.

The coupling between the spirals in this second configuration is shown in Fig. 8, demonstrating the same level of agreement between simulation and measurements. Again, ripples observed in the simulation seem to arise from unphysical reflection on the SM-ABC. Placing the boundary at even further distance, or using a PML truncation is expected to suppress a part of these ripples.

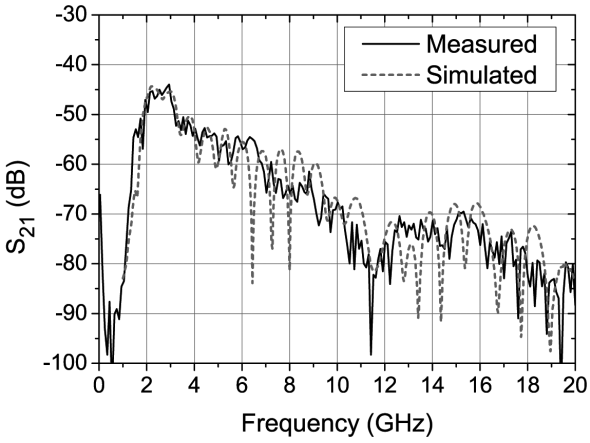

Fig. 8. Coupling parameter S_{21} of the two spirals in the tilted configuration of Fig. 7. The graph compares the results obtained from the FVTD simulations with measured data.

The results presented in this section have demonstrated that a great level of accuracy can be achieved through the use of a conformal time-domain method. This capability comes at a certain cost. In terms of memory requirements, the double spiral example benefits strongly from the modeling in an unstructured tetrahedral mesh. All presented simulations required between 2 and 3 GB memory, depending on the distance between the spirals. This can be regarded as a relatively modest cost considering the complexity of the models. However, the real limitation of the method is rather seen in the CPU time that is necessary to obtain the shown results. For the simulation to yield converging coupling parameters S_{21} over the whole considered frequency range, at least 12 ns have to be simulated. This is necessary in order to allow the low-frequency components of the pulse to propagate along the excited device

from the feed to the active (radiating) region of the spiral, to the second spiral, and there from the active region to the feed. Noting that the present FVTD code is not optimized for performance, the full simulation for the two spirals on a standard modern PC translates in CPU times in the order of days.

VI. Conclusion: assessment of the FVTD method

This paper has reviewed recent efforts in the development of cell centered FVTD algorithms, as a particular class of conformal time-domain methods. Several relevant aspects of a successful application of the method in microwave engineering have been addressed, and an advanced simulation example has been presented. This example has permitted to illustrate the strengths and drawbacks of the method.
On the side of the drawbacks, two aspects need to be mentioned. The first one concerns the dissipative nature of the flux-splitting algorithm. This puts an increased requirement on the maximal cell size that is required for a certain level of accuracy, and can degrade the results at higher frequencies. Alternative cell-centered algorithms that eliminate the dissipation at the expense of dispersion errors have not been proven to be reliable until now. Higher-order methods (e.g. [29],[30]) are often regarded as solution to the problem, however, introducing additional algorithmic complexity. The second problem of the FVTD method concerns the efficiency of the computation. This is directly associated with the spatial discretization using an unstructured mesh which inherently requires more operations per cell and per iteration step than a Cartesian grid. Nevertheless, this is not a critical problem because complex models with non-Cartesian structures typically require a smaller number of cells in an unstructured mesh compared to a regular grid. Due to this smaller number of cells, in order to achieve the same level of accuracy, the computational cost associated to the FVTD method can become lower in comparison to methods using Cartesian grids.
On the side of the strengths of the FVTD method, the most significant advantage is due to the geometrical flexibility of the algorithm. The example presented in this paper has clearly demonstrated the advantage of using inhomogeneous tetrahedral meshes which allows the modeling of very complex structures at a relatively modest memory cost. These results have been achieved with a straightforward explicit FVTD algorithm which naturally includes local mesh refinements. Furthermore, in the presented FVTD algorithm, all the field components are collocated both in space and time, which permits a very convenient treatment of boundaries, ports and sources. For improvement of the efficiency, the mesh inhomogeneity has been coupled to a geometry-matched local time-stepping scheme, which has been implemented as a fully automated procedure.
In conclusion, the authors are convinced that conformal time-domain methods, such as finite-volume or higher-order methods (e.g. Discontinuous Galerkin method), have a bright future in the landscape of electromagnetic simulation tools. The application of this class of methods as general-purpose field-solvers might be realized in standalone implementations. Yet hybridization with other numerical methods shows another promising way of taking advantage of the conformal algorithm potential in order to tackle the complexity of tomorrow's electromagnetic problems.

References

[1] Madsen, N.K.; Ziolkowski, R.W.: A three-dimensional modified finite volume technique for Maxwell's equations. Electromagnetics, **10** (1990), 147-161.

[2] Shankar, V.; Mohammadian, A.H.; Hall, W.F.: A time-domain, finite-volume treatment for the Maxwell equations. Electromagnetics, **10** (1990), 127-145.

[3] Bonnet, P.; Ferrieres, X.; Michielsen, B.L.; Klotz, P.; Roumiguières, J.L.: Finite-volume time domain method, Time domain electromagnetics, chapter 9, ed. by S.M. Rao, Academic Press, San Diego, 1999.

[4] Yee, K. S.; Chen, J.S.: The finite-difference time-domain (FDTD) and the finite-volume time-domain (FVTD) methods in solving Maxwell's equations. IEEE Trans. Antennas Propag., **AP-45** (1997), 354-363.

[5] Roe, P. L.: Approximate Riemann solvers, parameter vectors, and difference schemes. Journal of Computational Physics, **43** (1981), 357-372.

[6] Osher, S.; Chakravarthy, S.: High resolution schemes and the entropy condition. SIAM J. Numer. Anal., **21** (1984), 955-984.

[7] Baumann, D.; Fumeaux, C.; Vahldieck, R.: Field-based scattering-matrix extraction scheme for the FVTD method exploiting a flux-splitting algorithm. IEEE Trans. on Microw. Theory Tech., **MTT-53** (2005), 3595-3605.

[8] van Leer, B.: Towards the Ultimate Conservative Difference Scheme, V. A Second Order Sequel to Godunov's Method. J. Comp. Phys.., **32** (1979), 101-136.

[9] Warming, R. F.; Hyett, F.: The modified equation approach to the stability and accuracy analysis of finite-difference methods. Journal of Computational Physics, **14** (1974), 159-179.

[10] Warming, R. F.; Beam, R. M.: Upwind second-order difference schemes and applications in aerodynamic flows. AIAA J., **14** (1976), 1241-1249.

[11] Remaki, M.: A new finite volume scheme for solving Maxwell's system. COMPEL: The International Journal for Computation and Mathematics in Electrical and Electronic Engineering, **19** (2000), 913-931.

[12] Lohrengel, S.; Remaki, M.: A FV scheme for Maxwell's equations – Convergence analysis on unstructured meshes, 3rd symposium of finite volumes for complex applications, Porquerolles, France, June 24-28, 2002.

[13] Fromm, J. E.: A method for reducing dispersion in convective difference schemes. Journal of Computational Physics, **3** (1968), 176-189.

[14] Desideri, J. A.; Goudjo, A.; Selmin, V.: Third-order nu-

merical schemes for hyperbolic problems. Rapport de recherche INRIA no. 607, February 1987 (available from http://www.inria.fr/rrrt/rr-0607.html).

[15] Pacaud, D.: Développement de techniques différences finies – volumes finis performantes en électromagnétisme, PhD Thesis, University of Bordeaux I, France, 2001.

[16] Krohne, K.; Baumann, D.; Fumeaux, C.; Vahldieck, R.: Advances in the Application of Model Order Reduction to Finite Volume Models. Proceedings of Asia Pacific Microwave Conference, Delhi, India, December 2004.

[17] Krohne, K.; Baumann, D.; Vahldieck, R.: A State-Space Formulation for Field-Averaging Finite-Volume Models. Proceedings of International Zurich Symposium on Electromagnetic Compatibility, Singapore, March 2006.

[18] Wittig, T.; Munteanu, I.; Schuhmann, R.; Weiland, T.: Two Step Lanczos Algorithm for Model Order Reduction. IEEE Trans. Magn., **38** (2002), 673-676.

[19] Krohne, K.; Baumann, D.; Vahldieck, R.: Model Order Reduction for a Field-Averaging Finite-Volume Scheme. Proceedings of IEEE International Microwave Symposium, San Francisco, CA, USA, June 2006.

[20] Berenger, J. P.: A perfectly matched layer for the absorption of electromagnetic waves. Journal of Computational Physics, **114** (1994), 185-2004.

[21] Bonnet, F.; Poupaud, F.: Bérenger absorbing boundary condition with time finite-volume scheme for triangular meshes. Applied Numerical Mathematics, **25** (1997), 333-354.

[22] Sankaran, K.; Fumeaux, C.; Vahldieck, R.: Cell-centered finite-volume based perfectly matched layer for time-domain Maxwell system. IEEE Trans. Microw. Theory Tech., **54** (2006), 1269-1276.

[23] Sankaran, K.; Fumeaux, C.; Vahldieck, R.: Uniaxial and radial anisotropy models for finite-volume Maxwellian absorber. IEEE Trans. Microw. Theory Tech., **54** (12) (2006).

[24] Sankaran, K.; Kaufmann, T.; Fumeaux, C.; Vahldieck, R.: Different Perfectly Matched Absorbers for Conformal Time-Domain Method: A Finite-Volume Time-Domain Perspective, 23rd International Review of Progress in Applied Computational, Electromagnetics (ACES 2007), Verona, Italy, March 2007.

[25] Fumeaux, C.; Baumann, D.; Leuchtmann, P.; Vahldieck, R.: A generalized local time-step scheme for efficient FVTD simulations in strongly inhomogeneous meshes. IEEE Trans. on Microw. Theory Tech., **MTT-52**(3) (2004), 1067-1076.

[26] Bonnet, P.; Ferrieres, X.; Isaac, F.; Paladian, F.; Grando, J.; Alliot, J. C.; Fontaine, J.: Numerical modeling of scattering problems using a time domain finite volume method. Journal of Electromagnetic Waves and Applications, **11** (1997), 1165-1189.

[27] Ferrieres, X.; Parmantier, J. P.; Bertuol, S.; Ruddle, A. R.: Application of a Hybrid Finite Difference/Finite Volume Method to Solve an Automotive EMC Problem. IEEE Transactions on Electromagnetic Compatibility, **46** (2004), 624-634.

[28] Fumeaux, C.; Baumann, D.; Vahldieck, R.: Finite-Volume Time-Domain analysis of a cavity-backed Archimedean spiral antenna. IEEE Trans. Antennas and Propag., **AP-54** (2006), 844-851.

[29] Hesthaven, J. S.; Waburton, T.: Discontinuous Galerkin methods for the time-domain Maxwell's equations: An introduction. ACES Newsletter, **19** (2004), 10-29.

[30] Firsov, D.; LoVetri, J.; Jeffrey, I.; Okhmatovski, V.; Gilmore, C.; Chamma, W.: High-Order FVTD on Unstructured Grids using an Object-Oriented Computational Engine. ACES Journal, **22** (2007), pp. 71-82.

Christophe Fumeaux received the Diploma and Ph.D. degrees in physics from the ETH Zurich, Switzerland, in 1992 and 1997, respectively. From 1998 to 2000, he was a Post-Doctoral Researcher with the School of Optics, University of Central Florida, Orlando. In 2000, he joined the Swiss Federal Office of Metrology, Bern, Switzerland, as a Scientific Staff Member. Since 2001, he has been a Research Associate with the Laboratory for Electromagnetic Fields and Microwave Electronics (IFH), ETH, Zurich, Switzerland. During the Fall of 2005, he was a Visiting Scientist with the Laboratory of Sciences and Materials for Electronics, and of Automatic (LASMEA), University Blaise Pascal, Clermont-Ferrand, France. His current main research interest concerns computational electromagnetics in the time domain for numerical analysis of microwave circuits and antennas. Dr. Fumeaux has been the chairman of the IEEE Swiss Joint Chapter on Microwave Theory and Techniques, Antennas and Propagation, and EMC since January 2006. He was the recipient of the ETH Silver Medal of Excellence for his doctoral dissertation. He was the corecipient of the outstanding paper award of the Applied Computational Electromagnetics Society (ACES) in 2004.

Dirk Baumann received the Dipl. Ing. degree in electrical engineering from the University of Karlsruhe, Germany in 2001, and the Ph.D. degree in electrical engineering at the ETH Zurich, Switzerland in 2006. During the spring and fall of 2000, he held an internship with the Alaska SAR Facility (ASF), Fairbanks, Alaska, where he was involved with the calibration of ASF's SAR processor. In 2006, he was a post-doctoral researcher at the ETH Zurich involved in developments of the FVTD method, as well as in investigations of coil designs for 7T magnetic-resonance imaging (MRI). In 2007 he joined the Institute of High Performance Computing (IHPC), Singapore, as a Research Engineer. His current research interests include numerical methods with emphasis on time domain techniques.

Dr. Baumann was the recipient of the ETH Silver Medal of Excellence for his doctoral dissertation. He was the corecipient of the outstanding paper award of the Applied Computational Electromagnetics Society (ACES) in 2004.

Krishnaswamy Sankaran received the B.Eng. degree (with a first-class distinction) in electrical and electronics engineering from the University of Madras, Madras, India, in 2002, the M.Sc. degree in information and communication engineering from the University of Karlsruhe, Germany, in 2004, and is currently working toward the Ph.D. degree from the ETH Zurich, Zurich, Switzerland. From October 2003 to May 2004, he was a Research Trainee with the European Commission, Joint Research Centre, Ispra, Italy, where he was involved in the field of radar systems engineering and remote sensing. In June 2004, he joined the ETH Zurich, where he is currently with the Laboratory for Electromagnetic Field Theory and Microwave Electronics (IFH). His main research interests are numerical methods for solving EM field problems, computational physics, and applied mathematics.

In January 2007, he was invited by the Isaac Newton Institute for Mathematical Sciences, University of Cambridge, Cambridge, UK. Mr. Sankaran is currently vice-chair of the IEEE Student Branch Zürich. He was the recipient of a full postgraduate scholarship and he was one of the recipients of the 2006 Best Student Paper Award presented at the IEEE Microwave Theory and Techniques Society International Microwave Symposium, San Francisco, CA.

Rüdiger Vahldieck received the Dipl.-Ing. and Dr.-Ing. degrees in electrical engineering from the University of Bremen, Bremen, Germany, in 1980 and 1983, respectively. From 1984 to 1986, he was a Post-Doctoral Fellow with the University of Ottawa, Ottawa, ON, Canada. In 1986, he joined the Department of Electrical and Computer Engineering, University of Victoria, Victoria, BC, Canada, where he became a Full Professor in 1991. During the fall of 1992 and the spring of 1993, he was a Visiting Scientist with the Ferdinand-Braun-Institute für Hochfrequenztechnik, Berlin, Germany. In 1997, he became a Professor of EM-field theory with the ETH Zurich, Zurich, Switzerland, and Head of the Laboratory for Electromagnetic Fields and Microwave Electronics (IFH) in 2003. His research interests include computational electromagnetics in the general area of electromagnetic compatibility (EMC) and, in particular, for computer-aided design of microwave, millimeter-wave, and opto-electronic integrated circuits. Since 1981, he has authored or coauthored over 300 technical papers in books, journals, and conferences, mainly in the field of microwave computer-aided design. Prof. Vahldieck is the past president of the IEEE 2000 International Zurich Seminar on Broadband Communications (IZS2000). Since 2003, he has been president and general chairman of the International Zurich Symposium on Electromagnetic Compatibility. He is a member of the Editorial Board of the IEEE TRANSACTIONS ON MICROWAVE THEORY AND TECHNIQUES. From 2000 to 2003, he was an associate editor for the IEEE MICROWAVE AND WIRELESS COMPONENTS LETTERS, and from July 2003 until the end of 2005, he was the editor-in-chief. Since 1992, he has served on the Technical Program Committee (TPC) of the IEEE Microwave Theory and Techniques Society (IEEE MTT-S) International Microwave Symposium (IMS), the IEEE MTT-S Technical Committee on Microwave Field Theory, and in 1999, on the TPC of the European Microwave Conference. From 1998 to 2003, he was the chapter chairman of the IEEE Swiss Joint Chapter on Microwave Theory and Techniques, Antennas and Propagation, and EMC. Since 2005, he has been president of the Swiss Research Foundation on Mobile Communications. He was the recipient of the J. K. Mitra Award of the Institution of Electronics and Telecommunication Engineers (IETE) (in 1996) for the best research paper in 1995 and was corecipient of the Outstanding Publication Award of the Institution of Electronic and Radio Engineers in 1983. He was the corecipient of the 2004 Applied Computational Electromagnetic Society (ACES) Outstanding Paper Award.

Klaus Krohne received his Dipl.-Ing. degree in electrical engineering from the Darmstadt University of Technology in Germany in 2002 and a Dr. sc. degree from the Swiss Federal Institute of Technology, Zurich, Switzerland in 2007. He is currently a research engineer at the A-Star Institute for High Performance Computing in Singapore. His research interests include Computational Electromagnetics, Numerics, and Optimization of electromagnetic devices.

Erping Li received the B.Sc. degree from Hebei University of Technology, Tianjin, China, in 1983 and M.Sc. degree from Xi'an Jiaotong University, China, in 1986, and Ph.D. degree from Sheffield Hallam University, U.K, in 1992, all in electrical engineering. From 1989-1990, he worked as a Research Associate and 1991-1992 as a Research Fellow with the School of Electronic and Information Technology at Sheffield Hallam University, U.K. Between 1993 to 1999, he was a Senior Research Fellow, Principal Research Engineer and Technical Director with the Singapore Research Institute and Industry. Since 2000, he has been with Singapore National Institute of High Performance Computing, where he is currently a Senior Scientist and Senior R&D Manager of the Electronic Systems and Electromagnetics and the adjunct professor at National University of Singapore. Dr. Li authored and co-authored over 120 papers in the referred international journals and conferences and 5 book chapters. He holds and filed number of patents at US patent office. His research interests include fast and efficient computational electromagnetics, EMC/EMI, electromagnetics for nanoelectronics &RFIC, and bioelectromagnetics.

Dr Li is the recipient of 2006 IEEE EMC Technical Achievement Award, and the IEEE Certificate of Appreciation for his outstanding contribution to 2006 EMC-Zurich in Singapore as the conference chair. He has been elected as the IEEE Distinguished Lecturer for 2007-2008. Since January 2006, he serves as the Associate Editor for IEEE Microwave and Wireless Components Letters, was Guest Editor for IEEE Transactions on EMC November 2006 Special Issue. He served as the Symposium President for 2006 EMC-Zurich in Singapore and the Chairman of IEEE EMC Singapore Chapter for 2005-2006. He has been invited to give numerous speeches to academic institutions and international conferences.